The Role of Nonlinear C_{out} in Continuous Class F PAs

Y. Mary Asha Latha[#1], Luís C. Nunes[#2], Filipe M. Barradas[#3], José C. Pedro[#4]
[#] Instituto de Telecomunicações, Campus Universitário de Santiago, Aveiro, Portugal
[1]ymashalatha@ieee.org, [2]cotimos@ua.pt, [3]filipebarradas@ua.pt, [4]jcpedro@ua.pt

***Abstract*—This paper provides a comprehensive analysis of the role played by the equivalent nonlinear output capacitor (C_{out}), seen at the transistor's intrinsic drain, in the efficiency of continuous class F (CCF) power amplifiers (PAs). New design equations of the CCF PA are derived to incorporate the effect of this capacitance. It is noted that the nonlinearity of C_{out} can impose both active and passive second harmonic terminations at the current-source reference plane (CRP). A design methodology is proposed to obtain the optimum, passive, second harmonic terminations that maximize efficiency at the load reference plane (LRP). Finally, this improved design methodology is validated with experimental tests made on a CCF PA prototype.**

***Keywords*—Continuous class F, power amplifier (PA), nonlinear capacitor, nonlinear analysis.**

I. Introduction

Harmonic tuning is a popular technique in power amplifier (PA) design to achieve high efficiency [1]. The continuous class F (CCF) PA was introduced to maintain the output power and efficiency of Class F over a continuous design space [2-3]. Mapping the impedances from this space to frequency enables the design of broadband PAs. The CCF design equations are defined at the current-source reference plane (CRP) [3-4]. However, real transistors with a nonlinear output capacitance (C_{out}), see their waveforms altered from the ideal ones, so that the actual performance of the CCF PA at the load reference plane (LRP) is no longer optimum. Some previous studies on continuous class J (CCJ) PAs have presented the impedances and the performance of the PA at the LRP due to the nonlinear C_{out} [5-6]. Depending upon the required second harmonic impedance of the CCJ at the CRP, the resultant LRP impedance should be either active or passive. Moreover, the efficiency at the LRP is not constant within the design space, unlike the one measured at the CRP. An active CRP second harmonic load was also reported in CCF PAs with nonlinear C_{out} [4]. Although these studies have already presented the performance of the PA at the LRP, the reason behind the observed variation in the efficiency, and its relation to the active and passive nature of the CRP impedances is yet to be addressed. In fact, the design equations of CCF already found in the literature do not account for the effect of the nonlinear C_{out}.

To fill this gap, this paper analyzes the impact of a nonlinear C_{out} in CCF PAs. The design equations of the CCF PA are rewritten at both the CRP and the LRP, to include the effect of the nonlinear C_{out}. It follows from this new analysis that the second harmonic impedance needs to be considered active or passive at the CRP, unlike purely reactive, as predicted by the conventional CCF design. Consequently, a new design methodology to select the optimum passive impedance to place at the LRP for maximizing efficiency is proposed.

II. Design Equations of CCF PA with Nonlinear C_{out}

A. Theory of CCF PA

The drain-source voltage for CCF operation is [3-4],

$$v_{DS}(\theta) = (1-\alpha\cos\theta)^2(1+\beta\cos\theta)(1-\gamma\sin\theta) \quad (1)$$

where $\theta \equiv \omega_0 t$ and ω_0 is the excitation's angular frequency. Equation (1) results in the normalized (to $V_{ds0} = V_{DD}$) voltage waveform components,

$$V'_{ds1} = \frac{V_{ds1}}{V_{ds0}} = -\left[\frac{-(3\alpha^2\beta-8\alpha+4\beta)}{2\alpha^2-4\alpha\beta+4}\right] - j\gamma\left[\frac{1}{2}+\frac{2}{2\alpha^2-4\alpha\beta+4}\right] \quad (2)$$

$$V'_{ds2} = \frac{V_{ds2}}{V_{ds0}} = -\left[\frac{2}{\alpha^2-2\alpha\beta+2}-1\right] - j\gamma\left[\frac{(\alpha^2\beta-4\alpha+2\beta)}{2\alpha^2-4\alpha\beta+4}\right] \quad (3)$$

$$V'_{ds3} = \frac{V_{ds3}}{V_{ds0}} = \left[\frac{\alpha^2\beta}{2\alpha^2-4\alpha\beta+4}\right] - j\gamma\left[\frac{1}{2}-\frac{2}{2\alpha^2-4\alpha\beta+4}\right] \quad (4)$$

$$V'_{ds4} = \frac{V_{ds4}}{V_{ds0}} = -j\frac{\alpha^2\beta\gamma}{4(\alpha^2-2\alpha\beta+2)} \quad (5)$$

Accordingly, the normalized (to the peak current I_{max}) current waveform is defined as [4],

$$\frac{i_{DS}(\theta)}{I_{max}} = \frac{1}{\pi}+\frac{1}{2}\cos\theta+\frac{2}{3\pi}\cos 2\theta-\frac{2}{15\pi}\cos 4\theta+\frac{2}{35\pi}\cos 6\theta \quad (6)$$

and is fixed for any set of the voltage waveform parameters α, β, and γ. These equations can be recast by making $\beta = \alpha/\beta_1$, which allows quick assessment of the resistive part of the second harmonic impedance. For instance, in the conventional CCF PA the second harmonic impedance is purely reactive, which can be obtained by making $\beta_1 = 2$, or $\beta = \alpha/2$.

The maximum efficiency is found by maximizing $Re\{V'_{ds1}\}$ with α. For $\beta_1 \approx 2$, this can be achieved by maximizing the numerator, resulting in

$$\alpha \approx \frac{2\sqrt{2\beta_1-1}}{3} \quad (7)$$

The general practice to design a CCF PA is to enforce the voltage, and current equations defined in (1) and (6) at the CRP and create a design space that is then mapped to frequency by making use of γ, i.e., varying it within $[-1,1]$, since this parameter does not affect either efficiency or output power.

B. Theory of the CCF PA with Nonlinear C_{out}

The simplified model of a transistor with a nonlinear C_{out} is shown in Fig. 1 (a). The gate is assumed to be terminated by a short circuit at all harmonics, therefore, C_{out} represents the combination of the drain-source capacitor, C_{ds}, and the gate-drain capacitor C_{gd}, as in [5]. For a GaN HEMT, the nonlinear C_{out}, as a function of $v_{DS}(\theta)$, is well approximated by

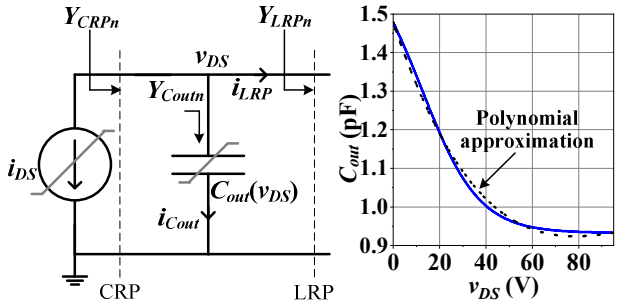

Fig. 1. (a) Simplified model of a transistor with nonlinear C_{out}, and (b) Nonlinear C_{out} as a function of $v_{DS}(\theta)$ of CCF PA.

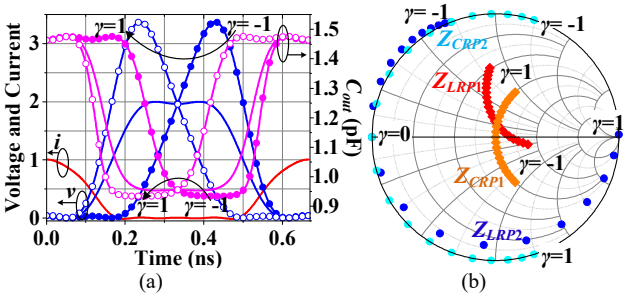

Fig. 2. (a) Normalized CRP voltage and current, and nonlinear C_{out} waveforms, and (b) Impedances of CCF PA at CRP and LRP planes.

$$C_{out}[v_{DS}(\theta)] = C_0 + \frac{A_c}{2}\left[1 - \tanh\left(K_c\left(V_c - v_{DS}(\theta)\right)\right)\right] \quad (8)$$

where C_0=0.93 pF, A_c= 0.74 pF, K_c= -0.04 V^{-1}, and V_c=12.58 V, for the 10 W GaN HEMT CGH40010F, which will be used for the PA implementation in this paper. Although C_{gd} varies with $v_{DG} = v_{DS} - v_{GS}$, its dependence on the gate-source voltage v_{GS} is neglected in this model as v_{GS} is much smaller than v_{DS}. The variation of the nonlinear C_{out} as a function of v_{DS} is shown in Fig. 1(b). With a nonlinear C_{out}, the output power and drain efficiency (DE) will be altered at the LRP. Beyond C_{out}, all elements are linear, and thus the performance at the package plane is similar to the one at the LRP, assuming low losses.

The time-domain waveform of C_{out} can be obtained by using (1) in (9), leading to the C_{out} waveforms shown in Fig. 2(a) along with the CRP voltage and current. The performance of the PA at the LRP can be calculated using the current at this plane, i_{LRP}. The current flowing through C_{out} is [7],

$$i_{Cout}(\theta) = C_{out}[v_{DS}(\theta)]\frac{dv_{DS}(\theta)}{d\theta} \quad (9)$$

and $i_{LRP} = -(i_{DS} + i_{Cout})$. Actually, i_{Cout} can be recast as,

$$i_{Cout}(\theta) = \frac{1}{2}\left[\sum_{n_1=0}^{N}\left(C_{outn_1}e^{jn_1\theta} + C^*_{outn_1}e^{-jn_1\theta}\right)\right] \times \frac{1}{2}\left[\sum_{n_2=0}^{N}\left(jn_2\theta V_{dsn_2}e^{jn_2\theta} - jn_2\theta V^*_{dsn_2}e^{-jn_2\theta}\right)\right] \quad (10)$$

in which $C_{out,n}$ are the Fourier components of $C_{out}[v_{DS}(\theta)]$. $V_{ds,n}$ are the Fourier components of $v_{DS}(\theta)$ given in (2)-(5). The fundamental and second harmonic components of the current i_{Cout} can be obtained from (10) as follows:

$$I_{Cout1} = j\omega_0 C_{out0}V_{ds1} - \frac{j\omega_0 C_{out2}V^*_{ds1}}{2} + \frac{j2\omega_0 C^*_{out1}V_{ds2}}{2} \ldots \quad (11)$$

$$I_{Cout2} = \frac{j\omega_0 C_{out1}V_{ds1}}{2} + j2\omega_0 C_{out0}V_{ds2} - \frac{j\omega_0 C_{out3}V^*_{ds1}}{2} \ldots \quad (12)$$

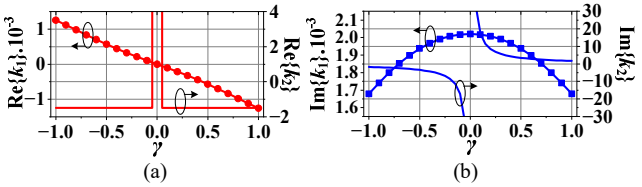

Fig. 3. Variation of the (a) real and (b) imaginary of k_1 and k_2 with γ.

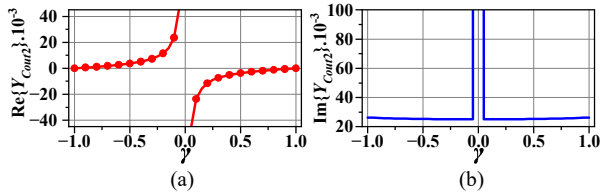

Fig. 4. Variation of (a) Real, and (b) Imaginary terms of Y_{Cout2} with γ.

The admittance seen at the LRP can now be obtained as

$$Y_{LRPn} = \frac{1}{Z_{LRPn}} = \frac{I_{LRPn}}{V_{dsn}} = -\frac{I_{dsn}+I_{Coutn}}{V_{dsn}} = Y_{CRPn} - Y_{Coutn} \quad (13)$$

Now Y_{LRPn} and Y_{CRPn}, for the CCF PA, at the fundamental and second harmonic, can be obtained by making β_1=2 and -1≤γ≤1 in (1)-(13), the result is shown in Fig. 2(b). When β_1=2 and γ=0, V_{ds2}=0, i.e., the CRP is a short circuit at the second harmonic, which enforces a short circuit on C_{out} and therefore, at the LRP. However, Y_{LRP2} is active for -1≤γ<0 and passive for 0<γ≤1, as shown in Fig. 2(b), this is analysed further in the next section.

III. Impact of the Nonlinear C_{out} on the CCF PA

A. Understanding the Nature of the LRP Admittances

The required Y_{LRP2} to enforce a purely susceptive Y_{CRP2}, is dependent on $Y_{Cout2} = \frac{I_{Cout2}}{V_{ds2}}$, as per (13). The second harmonic current I_{Cout2} through C_{out} can be approximated by the first two terms of (12), thus:

$$Y_{Cout2} \approx \underbrace{\frac{j\omega_0 C_{out1}}{2}}_{k_1}\cdot\underbrace{\frac{V_{ds1}}{V_{ds2}}}_{k_2} + j2\omega_0 C_{out0} \quad (14)$$

The nature of Y_{LRP2}, i.e., whether active or passive, is determined by the real part of Y_{Cout2}. Since C_{out0} is real, the second term of (14) is imaginary, therefore, $Re\{Y_{Cout2}\}$ only depends on the first term in (14), in particular in the products $Re\{k_1\}\cdot Re\{k_2\}$ and $-Im\{k_1\}\cdot Im\{k_2\}$. The variation of k_1 and k_2 with γ is shown in Fig. 3. The variation of k_1 with γ depends on C_{out1}, to obtain the dependence of C_{out1} on γ, (8) is first approximated by a 3rd order polynomial of v_{DS}, (15). This approximation of $C_{out}[v_{DS}]$ is shown in Fig. 1(b) (black dots).

$$C_{out}[v_{DS}(\theta)] \approx p_0 + p_1 v_{DS} + p_2 v_{DS}^2 + p_3 v_{DS}^3 \quad (15)$$

where p_0=1.48 pF, p_1= -1.79×10^{-2} pFV^{-1}, p_2=1.86×10^{-4} pFV^{-2} and p_3= -6.13×10^{-7} pFV^{-3}, for this case.

Now, by substituting the Fourier coefficients of v_{DS} in (15), C_{out1} can be approximated by:

$$C_{out1} \approx [p_1 V_{ds1} + 2p_2 V_{ds0}V_{ds1} + 3p_3 V_{ds0}^2 V_{ds1}] \quad (16)$$

In (16), p_1, p_2, and p_3 are constants, and $V_{ds0} = V_{DD}$, is also a constant. However, $Im\{V_{ds1}\}$ varies its sign with γ as per (2). Therefore, a similar change in sign can also be seen in $Re\{k_1\}$,

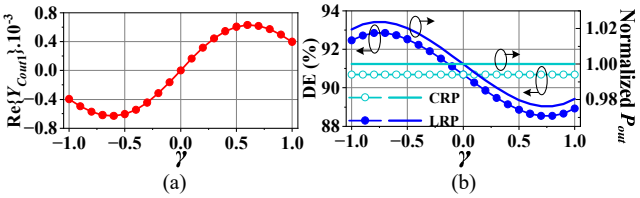

Fig. 5. Variation of (a) real of Y_{Cout1}, and (b) drain efficiency and normalized output power (P_{out}) at CRP and LRP with γ.

as shown in Fig. 3(a). Similarly, as $Im\{V_{ds1}\}$ and $Im\{V_{ds2}\}$ vary their sign with γ as per (2)-(3), a similar change in sign can also be seen in $Im\{k_2\}$, as shown in Fig. 3(b). Therefore, based on the different terms of k_1 and k_2, $Re\{Y_{Cout2}\}$ is positive (passive) for -1≤γ<0 and negative (active) for 0<γ≤1, as shown in Fig. 4(a). For all cases, $Im\{Y_{Cout2}\}$ remains positive, as shown in Fig. 4(b). To enforce a purely susceptive second harmonic admittance Y_{CRP2} at the CRP, Y_{LRP2} should compensate for the effects of Y_{Cout2}. Therefore, Y_{LRP2} needs to be active for -1≤γ<0 and passive for 0<γ≤1, as shown in Fig. 2(b), to present the desired CCF terminations at the CRP.

B. Performance Analysis at the LRP

Even if the CCF terminations are ensured at the CRP, the CCF DE of 90.7% is altered at the LRP due to C_{out}. The fundamental current flowing through C_{out}, I_{Cout1}, affects the output power (P_{out}) and DE at the LRP, as follows:

$$DE_{LRP} = \frac{P_{out,LRP}}{P_{DC}} = \frac{0.5\mathrm{Re}\{V_{ds1}\times-(I_{ds1}+I_{Cout1})^*\}}{V_{DD}I_{ds0}} \quad (17)$$

The real part of the fundamental admittance Y_{Cout1} seen through the nonlinear C_{out} is shown in Fig. 5(a). $Re\{Y_{Cout1}\}$ is negative (active) for -1≤γ<0, and an active fundamental power will be injected by the nonlinear C_{out}. Therefore, P_{out} and DE at the LRP are higher than those of the CRP for -1≤γ<0, as shown in Fig. 5(b), i.e., power is converted from second harmonic to fundamental. When 0<γ≤1, $Re\{Y_{Cout1}\}$ is positive (passive); as a result, the fundamental power will be converted in the nonlinear C_{out}, mainly to the second harmonic. Therefore, P_{out} and DE are decreased at the LRP as compared to the CRP for 0<γ≤1, as shown in Fig. 5(b).

C. Design Methodology

Although higher DE_{LRP} can be achieved for -1≤γ<0, the required second harmonic termination Y_{LRP2} is active, as shown in Fig. 2(b), which cannot be implemented with a passive matching network. On the other hand, Y_{LRP2} for 0<γ≤1 is inside the Smith chart, and can be further pushed to the edge of the Smith chart to improve DE_{LRP}. In order to achieve optimum Y_{LRP2}, corresponding to the best DE_{LRP} using a passive matching network, γ and β_1 of (1) are simultaneously varied. β_1<2 corresponds to passive Y_{LRP2}, and reduces the DE at the CRP from the CCF value of 90.7% [3]. When β_1>2, Y_{LRP2} is active, and, therefore, DE increases at the CRP.

However, the nature of these terminations and DE gets altered with γ and β_1 at the LRP due to the nonlinear C_{out}. The contours of $|\Gamma_{LRP2}|$ and DE_{LRP} with different γ and β_1 are shown in Fig. 6. It can be seen in Fig. 6 (b) that an increase in β_1, increases DE_{LRP}. The best DE_{LRP} with passive matching

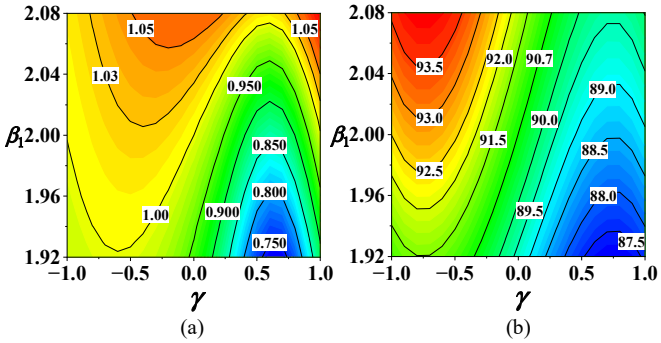

Fig. 6. Contours of (a) $|\Gamma_{LRP2}|$ and (b) drain efficiency at the LRP for different γ and β_1.

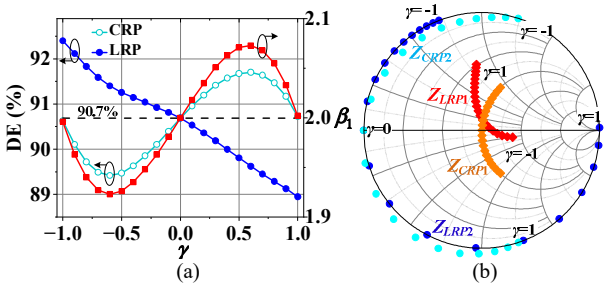

Fig. 7. (a) Mapping between γ and β_1, with corresponding DE, and (b) the CRP

network can be obtained when Y_{LRP2} is at the edge of the Smith chart, i.e., $|\Gamma_{LRP2}|$=1. For -1≤γ<0, $|\Gamma_{LRP2}|$=1 corresponds to β_1<2, as shown in Fig. 6 (a), whereas for 0<γ≤1, it is a β_1>2 that leads to a $|\Gamma_{LRP2}|$=1.

The mapping between γ and β_1 is crucial to achieve the best DE_{LRP} with a passive matching network. Based on the contours shown in Fig. 6, γ should be mapped to β_1, which corresponds to $|\Gamma_{LRP2}|$=1. The mapping between γ and β_1, and the resultant DE at the CRP and LRP are shown in Fig. 7 (a). The resulting impedances at CRP and LRP are shown in Fig. 7(b). Since -1≤γ<0 is mapped to β_1<2, DE at the CRP has reduced from the CCF value of 90.7%. However, due to the nonlinear C_{out}, the DE_{LRP} is higher than 90.7%. It can also be seen that Γ_{LRP2} is now moved from outside (Fig. 2 (b)) to the edge of the Smith chart and, therefore, can be achieved using a passive matching network. For 0<γ≤1, β_1>2 is selected, which has moved Γ_{LRP2} from inside (Fig. 2 (b)) to the edge of the Smith chart. This has improved the DE_{LRP} from that of the conventional CCF values shown in Fig. 5 (b). Note that the efficiency is above the CCF case at the LRP when it is below at the CRP, and vice-versa.

It can be seen from Fig. 7 (a) that the DE performance is not the same for different γ, and also that β_1=2, as proposed in the conventional CCF, is not optimal in real transistors with nonlinear C_{out}. This methodology finds the optimum, passive, fundamental and second harmonic terminations, for DE_{LRP}.

The third harmonic termination is also relevant for the design of the CCF PA. Here, it is considered as an open circuit, and its analysis was neglected. However, a similar analysis can be performed to obtain the optimum third harmonic termination, which is also impacted by the nonlinear C_{out}.

IV. Experimental Validation

To illustrate the proposed methodology, a CCF PA is designed using the 10 W GaN HEMT CGH40010F. A

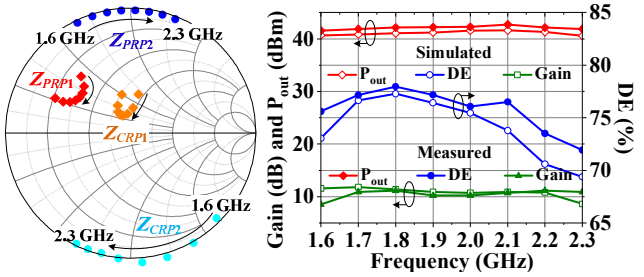

(a) (b)

Fig. 8. (a) CRP and PRP impedances of the designed CCF PA, and (b) Simulated and measured output power, DE, and gain at 3 dB compression.

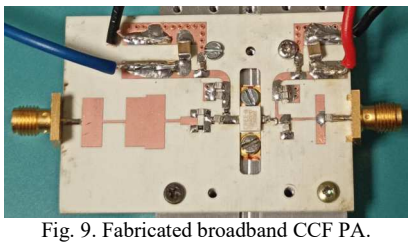

Fig. 9. Fabricated broadband CCF PA.

nonlinear embedding model is used to project the impedances from the CRP to the package reference plane (PRP). Based on the methodology presented in Section III-C, β_1>2 is selected for 0<γ≤1 to illustrate that the active CRP impedance can be achieved with a passive matching network. The fundamental and second harmonic impedances corresponding to β_1>2 and 0.5≤γ≤1 are mapped to frequencies from 1.6 to 2.3 GHz to design a broadband CCF PA. The third harmonic impedance is carefully placed to avoid a sudden drop in efficiency due to resonance, as in [4]. The second harmonic impedance at the gate terminal is placed near a short circuit, to also avoid resonance. The fundamental and second harmonic CRP and PRP impedances of the designed CCF PA are shown in Fig. 8 (a). It can be seen that the passive second harmonic impedance at the PRP is able to present an active impedance at the CRP. Unlike the conventional CCF, using β_1>2 in theory facilitated the appropriate choice of fundamental and active second harmonic impedance pair at the CRP.

The designed CCF PA was implemented on RO4350B substrate with a dielectric constant of 3.66 and thickness of 20 mil. The fabricated PA is shown in Fig. 9. The simulated and measured P_{out}, DE, and gain at 3 dB compression are shown in Fig. 8 (b). There is a good agreement between simulated and measured results in P_{out}, DE and gain, except for some deviation in the gain profile at the band edges. The final PA achieved a P_{out} of 41.6 to 42.7 dBm with DE of 72 to 78 %, with 8.6 to 11.1 dB gain at 3 dB compression for 1.6-2.3 GHz. The performance of the implemented PA is comparable to state-of-art continuous class PAs as shown in Table 1.

V. Conclusion

The impact of the nonlinear C_{out} on the performance of CCF PAs was analyzed by deriving the components of the CCF voltage that contribute to the power conversion from fundamental and second harmonic. By incorporating the nonlinear C_{out} in the design equations of CCF, the performance and impedance profile at the LRP could be predicted. The proposed methodology facilitated the design of a CCF PA with active CRP impedances using a passive matching network.

Table 1. Comparison with state-of-the-art continuous class PAs

Ref.	Freq. (GHz)	Efficiency (%)	Power (dBm)
[4]	1.45-2.45	70-81	40.4-42.2
[8]	0.55-0.92	70-80	39.3-41.1
[9]	1.5-2.9	60-76.5	39.4-41.9
[10]	1.5-2.5	60-70	39.5-40.5
[11]	1.3-3.3	60-83	40-40.4
This Work	1.6-2.3	72-78	41.6-42.7

References

[1] P. Colantonio, F. Giannini, and E. Limiti, *High Efficiency RF and Microwave Solid State Power Amplifiers*. Hoboken, NJ, USA: Wiley, 2009.

[2] F. H. Raab, "Class-F power amplifiers with maximally flat waveforms," *IEEE Trans. on Microw. Theory Techn.*, vol. 45, no. 11, pp. 2007-2012, Nov. 1997.

[3] V. Carrubba et al., "On the extension of the continuous class-F mode power amplifier," *IEEE Trans. on Microw. Theory Techn.*, vol. 59, no. 5, pp. 1294–1303, May 2011.

[4] N. Tuffy, L. Guan, A. Zhu and T. J. Brazil, "A Simplified Broadband Design Methodology for Linearized High-Efficiency Continuous Class-F Power Amplifiers," *IEEE Trans. Microw. Theory Techn.*, vol. 60, no. 6, pp. 1952-1963, June 2012.

[5] J. Moon, J. Kim and B. Kim, "Investigation of a Class-J Power Amplifier with a Nonlinear Cout for Optimized Operation," *IEEE Trans. Microw. Theory Techn.*, vol. 58, no. 11, pp. 2800-2811, Nov. 2010.

[6] Z. A. Mokhti, J. Lees, C. Cassan, A. Alt and P. J. Tasker, "The Nonlinear Drain–Source Capacitance Effect on Continuous-Mode Class-B/J Power Amplifiers," *IEEE Trans. on Microw. Theory Techn.*, vol. 67, no. 7, pp. 2741-2747, July 2019.

[7] L. C. Nunes, P. M. Cabral and J. C. Pedro, "AM/AM and AM/PM Distortion Generation Mechanisms in Si LDMOS and GaN HEMT Based RF Power Amplifiers," *IEEE Trans. on Microw. Theory Techn.*, vol. 62, no. 4, pp. 799-809, April 2014.

[8] V. Carrubba, J. Lees, J. Benedikt, P. J. Tasker, and S. C. Cripps, "A novel highly efficient broadband continuous class-F RFPA delivering 74% average efficiency for an octave bandwidth," *IEEE MTT-S Int. Microw. Symp. Dig.*, pp. 1–4, Jun. 2011.

[9] Y. M. A. Latha, K. Rawat and P. Roblin, "Nonlinear embedding model-based continuous class E/F power amplifier," *IEEE Microw. Wireless Comp. Lett.*, vol. 29, no. 11, pp. 714-717, Nov. 2019.

[10] P. Wright, J. Lees, J. Benedikt, P. J. Tasker and S. C. Cripps, "A Methodology for Realizing High Efficiency Class-J in a Linear and Broadband PA," *IEEE Trans. Microw. Theory Techn.*, vol. 57, no. 12, pp. 3196-3204, Dec. 2009.

[11] K. Chen and D. Peroulis, "Design of Broadband Highly Efficient Harmonic-Tuned Power Amplifier Using In-Band Continuous Class F^{-1}/F Mode Transferring," *IEEE Trans. Microw. Theory Techn.*, vol. 60, no. 12, pp. 4107-4116, Dec. 2012.